Nuclear Engineering and Technology 53 (2021) 1534–1539

Contents lists available at ScienceDirect

Nuclear Engineering and Technology

journal homepage: www.elsevier.com/locate/net

Original Article

Dissolution behavior of SrO into molten LiCl for heat reduction in used nuclear fuel

Dokyu Kang [a], James T.M. Amphlett [a], Eun-Young Choi [b], Sang-Eun Bae [b], Sungyeol Choi [a, *]

[a] Department of Nuclear and Quantum Engineering, Korea Advanced Institute of Science and Technology, 291 Daehak-ro, Yuseong-gu, Daejeon, 34141, Republic of Korea

[b] Korea Atomic Energy Research Institute, 111 Daedeok-daero 989, Yuseong-gu, Daejeon, 34057, Republic of Korea

ARTICLE INFO

Article history:
Received 3 August 2020
Received in revised form
12 November 2020
Accepted 20 November 2020
Available online 26 November 2020

Keywords:
Molten salt
Pyroprocessing
Fission products
Heat reduction process
Solubility

ABSTRACT

This study reports on the dissolution behavior of SrO in LiCl at varying SrO concentrations from low concentrations to excess. The amount of SrO dissolved in the molten salt and the species present upon cooling were determined. The thermal behavior of LiCl containing various concentrations of SrO was investigated. The experimental results were compared with results from the simulated results using the HSC Chemistry software package. Although the reaction of SrO with LiCl in the standard state at 650 °C has a slightly positive Gibbs free energy, SrO was found to be highly soluble in LiCl. Experimentally determined SrO concentrations were found to be considerably higher than those present in used nuclear fuel (<2 g/kg). As Sr-90 is one of the most important heat-generating nuclides in used nuclear fuel, this finding will be impactful in the development of fast, simple, and proliferation-resistant heat reduction processes for used nuclear fuel without the need for separating nuclear materials. Heat reduction is important as it decreases both the volume necessary for final disposal and the worker handling risk.

1. Introduction

The removal of radioactive isotopes that generate a large quantity of heat from used nuclear fuel (UNF) is an essential step before disposal or recycling [1,2]. High decay heat generation in UNF necessitates a larger disposal volume and increases the handling risk to workers [3–5]. For the first few centuries, heat generation is dominated by two fission products, Sr-90 and Cs-137. After 50 years of cooling, these two isotopes and their decay products still produce significant portions of the total UNF decay heat [6,7]. Sr-90 decays into Y-90, which subsequently decays into stable Zr-90. Both Sr-90 and Y-90 are beta-emitting radionuclides. Cs-137 undergoes beta decay into Ba-137 m, which then decays into stable Ba-137 through the emission of γ-rays.

One of the promising methods for the partitioning of these problematic radionuclides from UNF can be the dissolution of their oxides into molten salt. The dissolution of SrO, Cs_2O, and BaO were observed during the electrolytic oxide reduction of UNF [8–11]. Some researchers more thoroughly studied the reactions of alkali and alkaline earth metal oxides with molten salt [12–17]. Because the reactions of Cs and Ba oxides with LiCl are thermodynamically spontaneous, they are highly soluble in LiCl. In contrast, the reaction of SrO with LiCl at standard state at 650 °C has a positive Gibbs free energy, as shown in Table 1 [18].

Despite this thermodynamic limitation, SrO has been found to be soluble in LiCl. For example, Herrmann et al. [19,20] reported that Sr, Cs, and Ba oxides are soluble in the LiCl salt, showing an accumulation of Cs (690–719 ppm), Ba (620–630 ppm), and Sr (250 ppm) after six runs of electrolytic reduction were performed. W. Park et al. [21] carried out electrolytic reduction experiments using simulant oxide used nuclear fuel. They showed that 91.3% of Ba was dissolved from the fuel into LiCl salt, whereas only 66.8% of Sr was found in the salt. Although this significant amount of dissolution of SrO can be utilized to remove heat-generating SrO from UNF without separating nuclear materials from used fuel mixtures, no studies have yet examined the dissolution behavior of SrO in LiCl under various conditions and discussed its reaction mechanism.

This study investigates the dissolution behavior of SrO in LiCl at varying SrO concentrations from low to excess. The amount of SrO

* Corresponding author.
E-mail address: sungyeolchoi@kaist.ac.kr (S. Choi).

https://doi.org/10.1016/j.net.2020.11.019

Table 1
Gibbs free energy change for chlorination reactions of alkali and alkaline earth metal oxides with LiCl at 650 °C [18].

Reaction	Gibbs free energy change [kJ/mol]
$Cs_2O + 2LiCl \rightarrow 2CsCl + Li_2O$	−287.6
$BaO + 2LiCl \rightarrow BaCl_2 + Li_2O$	−55.5
$SrO + 2LiCl \rightarrow SrCl_2 + Li_2O$	1.517

dissolved in the molten salt was determined, as well as the species present upon cooling. The effect of increasing SrO dissolution on the thermal behavior of the salt was analyzed. Based on the experimental results, the mechanism of the SrO dissolution in LiCl at 650 °C was discussed. Finally, the equilibrium composition was derived and compared with those simulated using the HSC chemistry 10 software package.

2. Experimental

2.1. Materials

LiCl (anhydrous, > 99.9%) and SrO (anhydrous, > 99.5%) were purchased from Alfa-Aesar. HNO_3 (70%, purified by redistillation, ≥ 99.999% trace metals basis) was purchased from Sigma Aldrich. The anhydrous chemicals were stored in an Ar atmosphere glovebox ($[O_2]$, $[H_2O]$ < 5 ppm). LiCl was used as received in all experiments. Known amounts of SrO powder was pelletized into a cylindrical shape (diameter: 10.0 mm, height: 2.50–10.0 mm), using cold isostatic pressing (100 MPa) before use in the experiments. Alumina crucibles (≥99.8%) were purchased from SL SciLab.

2.2. Experimental setup

All the experiments were conducted in an electrical furnace integrated into a glovebox ($[H_2O]$, $[O_2]$ < 5 ppm). The specific experimental conditions are summarized in Table 2. SrO pellets and LiCl were loaded into an alumina cell at room temperature, and the cell was heated up to 650 °C, the typical operating temperature of the pyrochemical oxide reduction process [9,19,22]. Fig. 1. (a-1) shows the experimental configuration for the dissolution of SrO pellets in LiCl. The experimental cell consisted of LiCl, SrO pellets, and an alumina crucible (inner diameter: 32.0 mm, height: 29.0 mm, thickness: 3.50 mm). In Exp 6, a stainless-steel mesh basket (mesh size: 44 μm) was used to separate the undissolved SrO pellets and any suspended solids from the molten LiCl salt, as shown in Fig. 1. (b-1).

The cell was held at 650 °C for 3 h, followed by salt sampling using a stainless-steel ladle. A dissolution time of 3 h was considered adequate in Exp 1–4, based on our visual observations and literature reports for SrO dissolution [17]. However, in the case of Exp 5 and 6, some solid from the SrO pellet was observed even after 3 h of dissolution. To make sure that the reaction was not limited by the time, we held the cell 12 h more and then took the samples. Samples taken from Exp 1–4 were analyzed using Inductively Coupled Plasma Optical Emission Spectroscopy (ICP-OES), X-Ray Diffraction (XRD), Thermogravimetric Analysis-Differential Scanning Calorimetry (TGA-DSC), whereas only ICP-OES was used to analyze samples of Exp 5–6.

2.3. Analytical methods

ICP-OES (Agilent 5110), XRD (Rigaku SmartLab), and TGA-DSC (Setaram Labsys Evo) were used for sample analysis. The concentrations of Sr and Li in the samples were analyzed using ICP-OES (R^2 > 0.999 for calibration curve), and their phases at room temperature were identified using XRD. Because of the hygroscopic nature of the salt samples, they were loaded in an air-tight holder inside the glovebox to maintain inert conditions during the XRD measurement. The masses of XRD samples were controlled for the comparison of the relative amount of the species in the samples from the XRD peak ratios. For the TGA-DSC, samples were kept in argon-filled vials, and argon gas was purged into the device throughout the measurement. They were exposed to air only at the moment of sample loading on the equipment in an effort to minimize water ingress.

3. Results and discussion

3.1. Dissolution behavior of SrO into LiCl at 650 °C

The extent of the dissolution of SrO into LiCl was experimentally tested in Exp. 1–6. The concentrations of Sr in the samples, as determined using ICP-OES, are shown in Table 2. The concentrations of Sr in Exp. 1–4 were measured and found to be similar to the initial composition (dissolution = 97.34%–102.13%). Although there were small deviations between the theoretical maximum concentration of Sr and the value measured using ICP-OES, the deviations were sufficiently small (<2.66%) to be considered as systematic errors. Thus, it can be interpreted that all the SrO pellets were dissolved in LiCl in Exp 1–4, which is supported by the visual observation of the experimental cell (Fig. 1. (a-2)).

In contrast, the value was found to be 93.10% and 91.89% of the theoretical maximum in Exp 5 and 6, respectively. Although the experimental cell was held in the furnace for 15 h at 650 °C, the SrO pellets added to LiCl were not fully dissolved, as shown in Fig. 1. (a-3) and (b-2). This is a change in behavior when compared to the smaller SrO additions, suggesting that the solubility limit of SrO in molten LiCl has been reached. The concentrations of Sr in the samples from Exp 5 and 6 indicate that the solubility of SrO in LiCl at 650 °C can be estimated to be lower than 50.79 wt%.

The phases of solidified salt samples from Exp 1–4 were

Table 2
Experimental conditions and ICP-OES results of the dissolution experiments (Exp 1–6) in molten LiCl at 650 °C.

Exp. No.	Sampling time [h]	Initial salt composition				Conc. of Sr measured by ICP-OES [wt%]	Dissolution from initial SrO [%]
		Mass [g]		Conc. of SrO [wt%]	Conc. of Sr [wt%]		
		SrO	LiCl				
Exp 1	3	0.5	9.5	5.00	4.23	4.32 ± 0.15	102.13 ± 3.55
Exp 2	3	1.5	8.5	15.00	12.68	12.88 ± 0.08	101.58 ± 0.63
Exp 3	3	2.0	8.0	20.00	16.91	16.46 ± 0.35	97.34 ± 2.07
Exp 4	3	4.0	6.0	40.00	33.82	33.12 ± 0.36	97.93 ± 1.06
Exp 5	15	6.0	5.0	54.55	46.12	42.94 ± 0.20	93.10 ± 0.43
Exp 6[a]	15	6.0	5.0	54.55	46.12	42.38 ± 0.08	91.89 ± 0.17

[a] A Stainless steel mesh basket was used as a containment for SrO pellets to separate undissolved pellets from the salt.

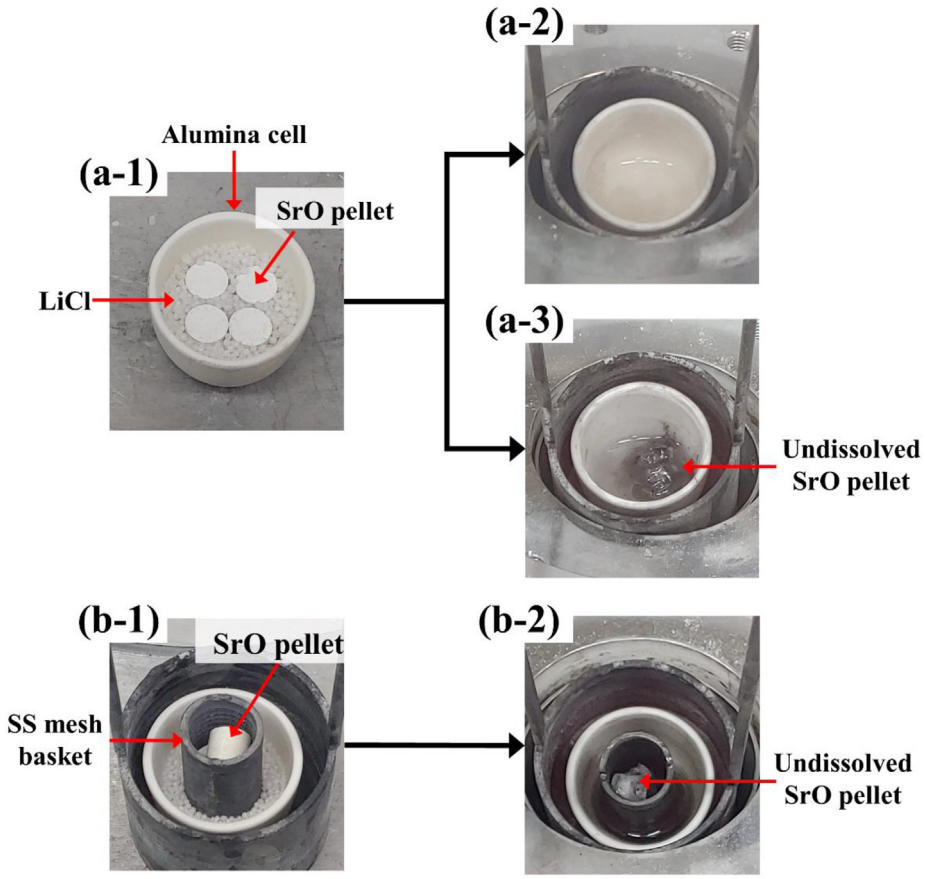

Fig. 1. Initial experimental configuration for (a-1) Exp 1–5, (b-1) Exp 6, status of the experimental cell at 650 °C for (a-2) Exp 1–4, (a-3) Exp 5, and (b-2) Exp 6.

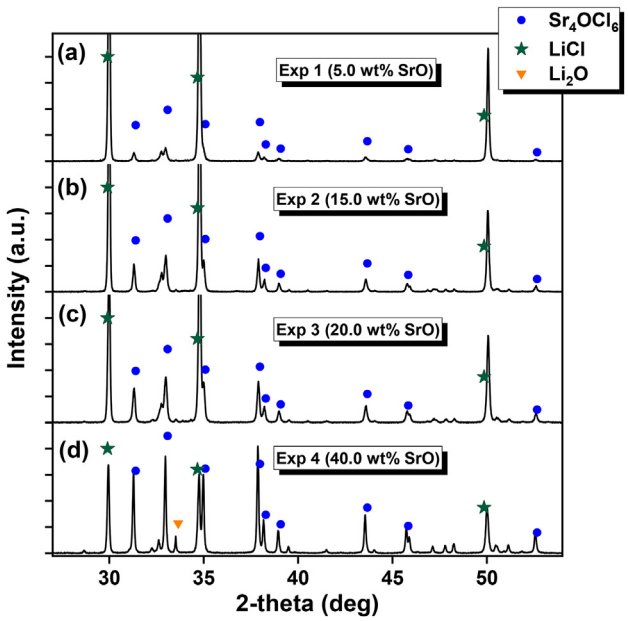

Fig. 2. XRD patterns of solidified salt samples from (a) Exp 1 (5.0 wt% of SrO), (b) Exp 2 (15.0 wt% of SrO), (c) Exp 3 (20.0 wt% of SrO), and (d) Exp 4 (40.0 wt% of SrO).

identified by XRD at room temperature (Fig. 2. (a)~(d)). Products of the dissolution reaction of SrO in molten LiCl are well illustrated in the collected XRD pattern of the most concentrated sample (Fig. 2. (d)), in which Sr_4OCl_6 and Li_2O phases, in addition to LiCl, were observed. However, another potential species in the samples, SrO, was not distinguishable because the peak patterns of the LiCl and SrO were overlapped due to their crystal structures possessing almost the same diffraction angles.

As the concentration of SrO in the LiCl increased, the intensity of the peak patterns corresponding to Sr_4OCl_6 and Li_2O increased together, while more LiCl was consumed by the dissolution reaction. Although the peak patterns of Li_2O are not visible in the results of samples from Exp 1–3 due to the relatively low amount of Li_2O, the intensity increased with the higher concentration of SrO. Based on these results, the overall behavior of SrO when undergoing dissolution and then subsequent quenching in LiCl can be expressed, as shown in Equation (1).

$$4SrO(s) + 6LiCl \rightleftharpoons Sr_4OCl_6 + 3Li_2O \quad (1)$$

The formation of alkaline earth metal oxychlorides in different molten salt environments has been reported in the literature [17,23,24]. Volkovich et al. [17] reported on the formation of the bulky anionic strontium oxychloride species when SrO was dissolved in the molten $SrCl_2$ salt, as described in Equation (2). Nikolaeva et al. [23,24] also investigated the dissolution mechanism of BaO in the $BaCl_2$, and they observed the formation of anionic barium oxychloride species in the molten salt using Raman spectroscopy as shown in Equation (3).

$$SrO(s) + SrCl_2 + (n-2)Cl^- \rightleftharpoons [Sr_2OCl_n]^{(n-2)-} \quad (2)$$

$$BaO(s) + [BaCl_6]^{4-} \rightleftharpoons [Ba_2OCl_6]^{4-} \quad (3)$$

Therefore, the formation of strontium oxychloride species is thought to be a reasonable explanation for the observed solubility of SrO in the molten LiCl. This speciation in the molten salt system arises from a different mechanism than $SrCl_2$ formation, meaning the Gibbs reaction energy will be different to the $SrCl_2$ case (Table 1), and in this case, likely negative.

3.2. Thermal behavior of LiCl–SrO system

The effect of increasing concentration of SrO in LiCl on the thermal behavior of the salt was investigated using TGA-DSC. The heat flows of pre-melted LiCl–SrO samples were monitored as the temperature increased to their melting points (Fig. 3), while the results of TGA were not shown here because the mass losses by the vaporization of the moisture in the samples were only observed. The DSC results for the temperature range between 50 °C and 300 °C were omitted for the same reason. The endothermic peaks indicating the melting of the samples appeared at temperatures over 400 °C.

As more SrO was added to the LiCl, both the solidus and the liquidus temperature of the samples occurred at lower temperatures (from the result of Exp 1 to that of Exp 4). The decrease in the melting point of LiCl containing SrO compared with that of pure LiCl salt (T_m = 605 °C) can be explained by eutectic melting between LiCl and SrO. Using the DSC results, the solidus and liquidus temperatures of the pre-melted LiCl–SrO samples were plotted in Fig. 4.

The eutectic melting point can be estimated to be lower than the liquidus temperature of the sample from Exp 4 ($T_{eutectic}$ < 488.46 °C), which seems to be similar to the eutectic melting point of LiCl–$SrCl_2$ ($T_m \approx$ 484 °C at 35.71 mol% of $SrCl_2$) [25]. In addition, the solubility of SrO can be derived from the liquidus composition because the liquidus composition corresponds to the saturated concentration of the solid phase in the liquid phase. From our DSC results, which showed 649.14 °C and 674.85 °C of the liquidus temperature at 24.63 mol% (44.39 wt%) and 29.69 mol% (50.79 wt%) of SrO, respectively, the solubility of SrO at 650 °C can be estimated to be between the two values (44.39 wt%~50.79 wt%), as shown in Fig. 4.

3.3. Reaction equilibrium for SrO dissolution

The equilibrium composition of the dissolution reaction described in Equation (1) was estimated by calculating the molar fraction of each species in the equation using the ICP-OES results.

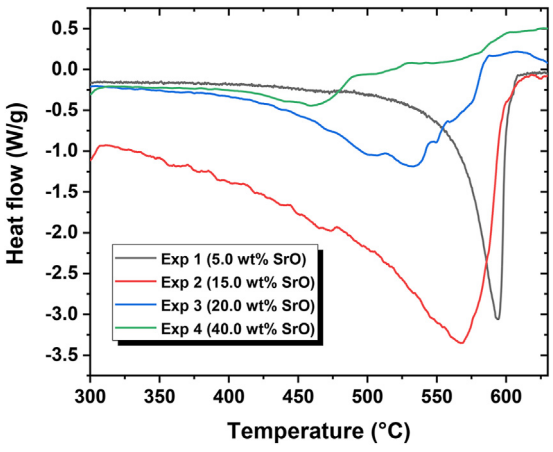

Fig. 3. DSC results of the pre-melted LiCl–SrO samples from Exp 1–4.

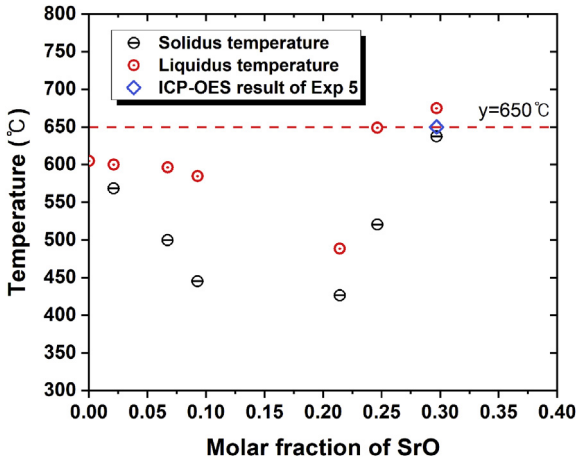

Fig. 4. Solidus and liquidus temperatures of pre-melted LiCl–SrO samples and the ICP-OES result of the sample from Exp 5.

Three assumptions were established for the derivation. First, the molar concentrations of Sr and Li obtained from the ICP-OES measurement are equal to the sum of the molar concentrations of each element in the reactants and products as described in Equations (4) and (5), respectively. Second, the ratio of molar concentrations of the products in Equation (1) is identical to that of the stoichiometric coefficients in Equation (1). Third, the sample mass is equal to the sum of the mass of each compound multiplied by the dilution volume (Equation (7)).

$$[Sr] = [SrO] + 4[Sr_4OCl_6] \quad (4)$$

$$[Li] = [LiCl] + 2[Li_2O] \quad (5)$$

$$[Sr_4OCl_6] = 3[Li_2O] \quad (6)$$

$$V\{M_{SrO}[SrO] + M_{LiCl}[LiCl] + M_{Sr_4OCl_6}[Sr_4OCl_6] + M_{Li_2O}[Li_2O]\} = m \quad (7)$$

where $[i]$ is the molar concentration of the species i (mol/L), M_i is the molar mass of the species i (g/mol), m is the mass of the sample (g), and V is the dilution volume of ICP-OES solution (L).

Solving the system of linear equations, Equations (4)–(7), the molar concentrations of each species in Equation (1) were obtained, as shown in Fig. 5. (a) and (b). As more SrO was added in LiCl, the molar fraction of SrO itself and the reaction products (Sr_4OCl_6 and Li_2O) increased, while the molar fraction of LiCl decreased. This trend is consistent with the change in the peak ratios in the XRD results, which showed the increasing and decreasing intensity of the peaks corresponding to the reaction products and LiCl, respectively. However, the increasing molar fraction of SrO estimated in Fig. 5 is still questionable because this trend was not observable in the XRD results due to the peak overlap between SrO and LiCl.

For the comparison with the chlorination reaction, the equilibrium for the reaction producing $SrCl_2$ was also estimated in the same way as for the Sr_4OCl_6, as shown in Fig. 5. (c) and (d) in which the simulated results were provided together from using HSC Chemistry 10. The simulation was conducted with different activity coefficients of SrO (γ_{SrO}= 0.1, 1.0, and 10), where an activity coefficient of 8.4 was used for Li_2O [26] while that of LiCl and $SrCl_2$ were set to 1 due to the absence of relevant data in the literature [27]. In the case of Sr_4OCl_6, the database entry does not exist in HSC

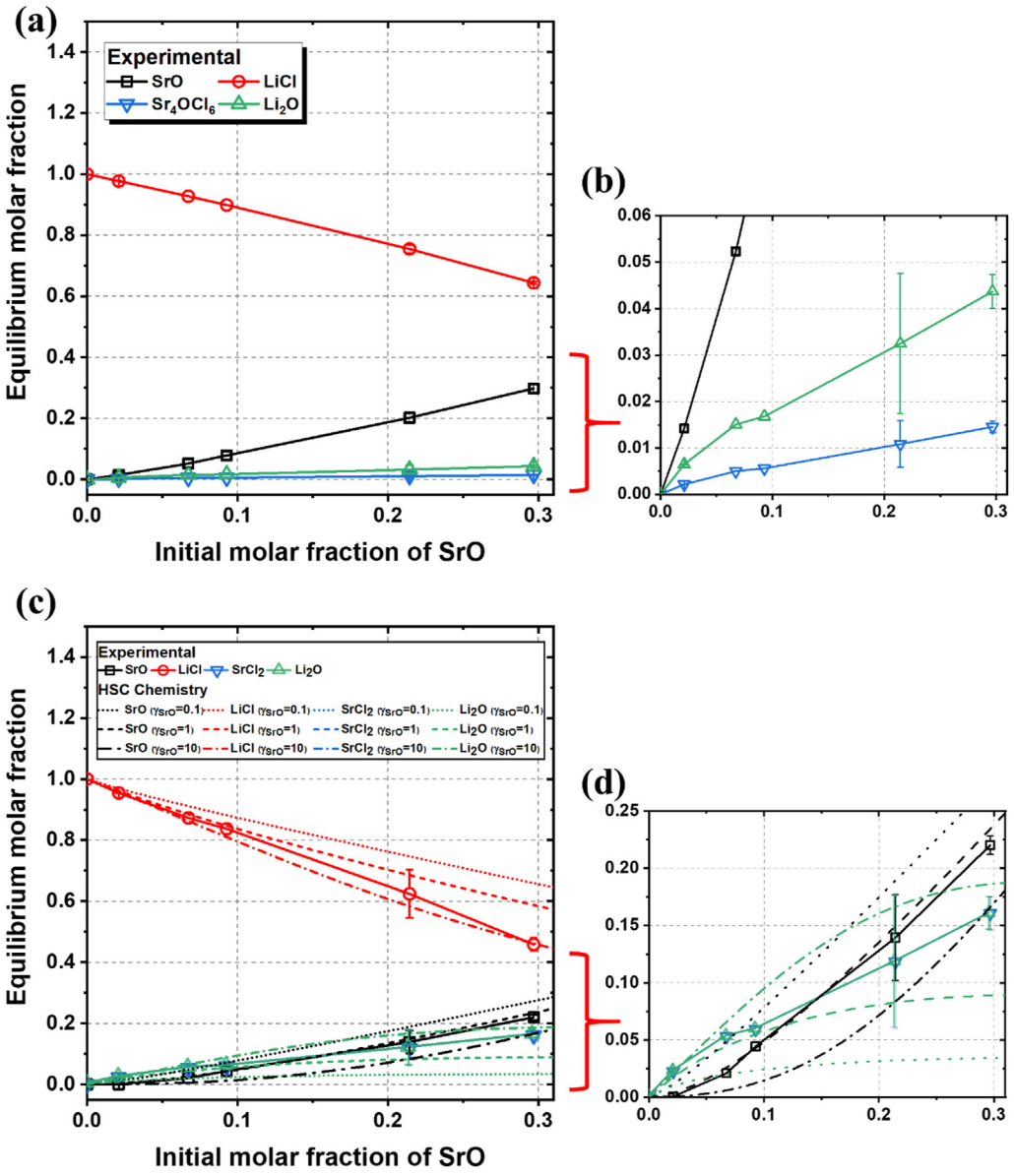

Fig. 5. Equilibrium molar fraction of each species in the reaction for (a) $4SrO+6LiCl \rightleftharpoons Sr_4OCl_6+3Li_2O$, (b) enlarged figure for the red highlighted region in the left figure, equilibrium molar fraction of each species in the reaction for (c) $SrO+2LiCl \rightleftharpoons SrCl_2+Li_2O$ (data represented by the dot, dash, and dash-dot lines corresponding to the result with $\gamma_{SrO} = 0.1$, $\gamma_{SrO} = 1$, and $\gamma_{SrO} = 10$, respectively, were derived from HSC Chemistry 10 software package simulation), and (d) enlarged figure for the red highlighted region in the left figure. (For interpretation of the references to colour in this figure legend, the reader is referred to the Web version of this article.)

Chemistry 10, so the results could not be provided.

Although the data points in Fig. 5 possessed the high deviations caused from the systematic errors from the scale and ICP-OES, and the moisture contained in the samples, the overall trend in the results of the chlorination reaction is not only similar to the results of the reaction producing Sr_4OCl_6 but also to the simulated results. At the low concentration of SrO, the simulated results with $\gamma_{SrO} = 1$ showed the most similar trend to the experimental results because the experimental setup was close to the ideal case. On the other hand, at the high concentration of SrO, the experimental results were located between the simulated results with $\gamma_{SrO} = 1$ and $\gamma_{SrO} = 10$. This result seems to be reasonable because the activity coefficient of SrO can vary with the surrounding enviornment. Considering the real condition in UNF, which is a mixture of UO_2 and fission products, the activity coefficient of SrO is expected to smaller than in our experimental setup, and the reaction will be less favorable, which is consistent with the results of the oxide reduction process conducted at Idaho National Laboratory [20].

4. Conclusions

This study reports on the unexpected high solubility of SrO in LiCl at 650 °C by observing the dissolution behaviors and reaction mechanisms of SrO at varying SrO concentrations. No solid phase was observed until 40.0 wt% of SrO in LiCl was reached, while a separate solid phase was noted at 54.55 wt%. In the case involving an excess of SrO, at 54.55 wt%, up to 50.79 wt% of SrO was observed in the solution phase. The amount of SrO dissolved in LiCl was much greater than the typical concentration (<2 g/kg) in UNF. The XRD patterns of pre-melted LiCl containing SrO at room temperature showed the presence of Sr_4OCl_6 in the quenched salt. In addition, the simulated results for the reaction of SrO and LiCl to form $SrCl_2$

and Li_2O at 650 °C were compared with the experimental results. Considering the relatively low solubility of SrO in $SrCl_2$ and Li_2O in LiCl, the high solubility of SrO in LiCl may be explained by an entropy-driven phenomenon. While reacting SrO with LiCl, it potentially forms $SrCl_2$ and Sr_4OCl_6 that form a eutectic with LiCl. In this complex eutectic, SrO may be soluble in LiCl and $SrCl_2$. This finding could be used to develop a fast, simple, and proliferation-resistant heat reduction process for UNF without the need for separating nuclear materials.

Declaration of competing interest

The authors declare that they have no known competing financial interests or personal relationships that could have appeared to influence the work reported in this paper.

Acknowledgements

This work was supported by the National Research Foundation of Korea (NRF) funded by the Ministry of Science and ICT (The grant number: NRF-2016M2B2B1945249).

References

[1] S. Choi, W. Il Ko, Dynamic assessments on high-level waste and low- and intermediate-level waste generation from open and closed nuclear fuel cycles in Republic of Korea, J. Nucl. Sci. Technol. 51 (2014) 1141–1153, https://doi.org/10.1080/00223131.2014.905804.
[2] S. Choi, H.O. Nam, W. Il Ko, Environmental life cycle risk modeling of nuclear waste recycling systems, Energy 112 (2016) 836–851, https://doi.org/10.1016/j.energy.2016.06.127.
[3] K. Ikonen, Thermal Analyses of Spent Nuclear Fuel Repository Thermal Analyses of Spent Nuclear Fuel Repository, 2003.
[4] H.S. Jung, S. Choi, I.S. Hwang, M.-J. Song, Environmental assessment of advanced partitioning, transmutation, and disposal based on long-term risk-informed regulation: PyroGreen, Prog. Nucl. Energy 58 (2012) 27–38, https://doi.org/10.1016/j.pnucene.2012.02.003.
[5] R. Gao, S. Choi, Y. Zhou, W. Il Ko, Performance modeling and analysis of spent nuclear fuel recycling, Int. J. Energy Res. 39 (2015) 1981–1993, https://doi.org/10.1002/er.3424.
[6] R.A. Wigeland, T.H. Bauer, T.H. Fanning, E.E. Morris, Separations and transmutation criteria to improve utilization of a geologic repository, Nucl. Technol. 154 (2006) 95–106, https://doi.org/10.13182/NT06-3.
[7] A.N. Williams, M. Pack, S. Phongikaroon, Separation of strontium and cesium from ternary and quaternary lithium chloride-potassium chloride salts via melt crystallization, Nucl. Eng. Technol. 47 (2015) 867–874, https://doi.org/10.1016/j.net.2015.08.006.
[8] E.J. Karell, R.D. Pierce, T.P. Mulcahey, Treatment OF oxide spent fuel using the lithium reduction process, Proc. Am. Nucl. Soc. Meet. 53 (1996) 1689–1699, https://doi.org/10.1017/CBO9781107415324.004.
[9] E.Y. Choi, S.M. Jeong, Electrochemical processing of spent nuclear fuels: an overview of oxide reduction in pyroprocessing technology, Prog. Nat. Sci. Mater. Int. 25 (2015) 572–582, https://doi.org/10.1016/j.pnsc.2015.11.001.
[10] S. Herrmann, S. Li, M. Simpson, Electrolytic reduction of spent light water reactor fuel bench-scale experiment results, J. Nucl. Sci. Technol. 44 (2007) 361–367, https://doi.org/10.1080/18811248.2007.9711295.
[11] W. Il Ko, H.H. Lee, S. Choi, S.-K. Kim, B.H. Park, H.J. Lee, I.T. Kim, H.S. Lee, Preliminary conceptual design and cost estimation for Korea advanced pyroprocessing facility plus (KAPF+), Nucl. Eng. Des. 277 (2014) 212–224, https://doi.org/10.1016/j.nucengdes.2014.06.033.
[12] V.L. Cherginets, T.P. Rebrova, V.A. Naumenko, On metal oxide solubilities in some molten alkali metal bromides at T = 973 K, J. Chem. Thermodyn. 74 (2014) 216–220, https://doi.org/10.1016/j.jct.2014.02.001.
[13] I.N.I. Solvents, Chapter 3 equilibria in "solid oxide-ionic melt" systems, compr, Chem. Kinet 41 (2005) 229–345, https://doi.org/10.1016/S0069-8040(05)80006-8.
[14] J. Jeon, J. Yeon, Y. Cho, I. Choi, W. Kim, Determination of oxide ion activity in molten LiCl using oxide ion electrode, Proc. Korean Nucl. Autumn Meet 2002 (2002).
[15] D.H. Kim, S.E. Bae, J.Y. Kim, T.H. Park, Y.J. Park, K. Song, Solubility measurement of Li2O in LiCl molten salt for electro-reduction process, Asian J. Chem. 25 (2013) 7055–7057, https://doi.org/10.14233/ajchem.2013.18.
[16] Y. Sakamura, Solubility of Li[sub 2]O in molten LiCl–MCl[sub x] (M=Na, K, Cs, Ca, Sr, or Ba) binary systems, J. Electrochem. Soc. 157 (2010) E135, https://doi.org/10.1149/1.3456631.
[17] A.V. Volkovich, M.V. Solodkova, Z.V. Zhukova, M.V. Sigailov, D.P. Vent, Interaction of strontium oxide with Sr-Cl2-MCl melts, Russ. Metall. 2011 (2011) 122–126, https://doi.org/10.1134/S0036029511020157.
[18] S.M. Jeong, B.H. Park, J.M. Hur, C.S. Seo, H. Lee, Ki-Chan Song, An experimental study on an electrochemical reduction of an oxide mixture in the advanced spent-fuel conditioning process, Nucl. Eng. Technol. 42 (2010) 183–192, https://doi.org/10.5516/NET.2010.42.2.183.
[19] S.D. Herrmann, S.X. Li, M.F. Simpson, S. Phongikaroon, Electrolytic reduction of spent nuclear oxide fuel as part of an integral process to separate and recover actinides from fission products, Separ. Sci. Technol. 41 (2006) 1965–1983, https://doi.org/10.1080/01496390600745602.
[20] S.D. Herrmann, S.X. Li, Separation and recovery of uranium metal from spent light water reactor fuel via electrolytic reduction and electrorefining, Nucl. Technol. 171 (2010) 247–265, https://doi.org/10.13182/NT171-247.
[21] W. Park, E.Y. Choi, S.W. Kim, S.C. Jeon, Y.H. Cho, J.M. Hur, Electrolytic reduction of a simulated oxide spent fuel and the fates of representative elements in a Li2O-LiCl molten salt, J. Nucl. Mater. 477 (2016) 59–66, https://doi.org/10.1016/j.jnucmat.2016.04.058.
[22] H. Lee, G. Il Park, J.W. Lee, K.H. Kang, J.M. Hur, J.G. Kim, S. Paek, I.T. Kim, I.J. Cho, Current status of pyroprocessing development at KAERI, Sci. Technol. Nucl. Install. 2013 (2013), https://doi.org/10.1155/2013/343492.
[23] E.V. Nikolaeva, I.D. Zakiryanova, I.V. Korzun, A.L. Bovet, B.D. Antonov, Interaction between barium oxide and barium containing chloride melt, Zeitschrift Fur Naturforsch. - Sect. A J. Phys. Sci. 70 (2015) 325–331, https://doi.org/10.1515/zna-2014-0370.
[24] E.V. Nikolaeva, I.D. Zakiryanova, A.L. Bovet, I.V. Korzun, On barium oxide solubility in barium-containing chloride melts, Zeitschrift Fur Naturforsch. - Sect. A J. Phys. Sci. 71 (2016) 731–734, https://doi.org/10.1515/zna-2016-0163.
[25] H.S. Lee, G.H. Oh, Y.S. Lee, I.T. Kim, E.H. Kim, J.H. Lee, Concentrations of CsCl and SrCl2 from a simulated LiCl salt waste generated by pyroprocessing by using czochralski method, J. Nucl. Sci. Technol. 46 (2009) 392–397, https://doi.org/10.3327/jnst.46.392.
[26] J.-M. Hur, S.M. Jeong, H. Lee, Underpotential deposition of Li in a molten LiCl–Li2O electrolyte for the electrochemical reduction of U from uranium oxides, Electrochem. Commun. 12 (2010) 706–709, https://doi.org/10.1016/j.elecom.2010.03.012.
[27] M.K. Jeon, S.-W. Kim, S.-K. Lee, E.-Y. Choi, Thermodynamic Calculations on the Chemical Behavior of SrO During Electrolytic Oxide Reduction, J. Nucl. Fuel Cycle Waste Technol. 18 (2020) 415–420.